

Effect of SiO₂, total FeO, Fe³⁺/Fe²⁺, and alkali elements in basaltic glasses on mid-infrared spectra

CÉLESTE D.M. DUFRESNE,^{1,*} PENELOPE L. KING,^{1,2} M. DARBY DYAR,³ AND KIM N. DALBY^{1,†}

¹Department of Earth Sciences, The University of Western Ontario, London, Ontario N6A 5B7, Canada

²Institute of Meteoritics, University of New Mexico, Albuquerque, New Mexico 87131, U.S.A.

³Department of Astronomy, Mount Holyoke College, South Hadley, Massachusetts, 01075, U.S.A.

ABSTRACT

A suite of basaltic glasses were examined to determine how subtle compositional changes affect mid-infrared spectra (650 to 5400 cm⁻¹). Glasses with different SiO₂, FeO_{total}, Fe³⁺/Fe²⁺, and alkali contents were synthesized in a gas-mixing furnace and analyzed using electron probe microanalysis, Mössbauer spectroscopy, and micro-reflectance Fourier transform infrared spectroscopy. The major mid-infrared spectral feature in silicate glasses is a broad peak located at ~900 to 1100 cm⁻¹ arising from Si-(Al)-O asymmetric stretching vibrational modes. To accurately compare spectra of different glass compositions, we have applied the Kramers-Kronig (KK) transform to our spectra and examined the resulting absorption peak (KK abs. peak). The location of the KK abs. peak shifts to higher wavenumbers as SiO₂ content increases (1031–1054 cm⁻¹ with SiO₂ from 47.18 to 55.57 wt%). For basaltic glasses with near-constant Al/(Al+Si), the full-width half maximum of the KK abs. peak decreases as alkali content increases (235–188 cm⁻¹ with Na₂O+K₂O contents from 0.07 to 3.74 wt%). In contrast, the location and shape of the KK abs. peak are not affected by variations in total FeO (6.06–16.30 wt%) and Fe³⁺/Fe²⁺ (0.05–1.17). Our results show that KK transformed mid-infrared spectra of basaltic glasses may be used to determine the SiO₂ contents in basaltic glasses, irrespective of FeO_{total} and Fe³⁺/Fe²⁺, and the alkali contents if Al/(Al+Si) is known. These observations will aid in the interpretation of laboratory and remotely sensed IR spectra.

Keywords: IR peak location and shape, glass composition, Mössbauer spectroscopy, oxygen fugacity

INTRODUCTION

Tholeiitic basalt is the most common terrestrial volcanic rock type and is also ubiquitous on other planetary bodies (Basaltic Volcanism Study Project 1981). Tholeiitic basalts may be dominated by basaltic glass; for example, on the Earth's seafloor, and presumably on cold, atmosphere-poor planets where molten material quenched to form glass or where impact processes have melted basaltic rocks. To determine the composition of basaltic materials remotely, many workers have used infrared (IR) spectroscopy (e.g., Hunt et al. 1950; Salisbury and Wald 1992; Clark 1999; Christensen et al. 2000; Wyatt et al. 2001). However, there are relatively few laboratory studies of basaltic glasses (Crisp et al. 1990; Minitti et al. 2002, 2005; Johnson et al. 2007) and only a small number of emission IR measurements of glasses (e.g., Christensen et al. 2000; Wyatt et al. 2001; Johnson et al. 2003, 2007; Minitti et al. 2006, 2007). Therefore, our understanding of the relationship between glass composition and IR spectra is limited.

In mid-IR spectroscopy, the major spectral feature(s) observed in most silicate minerals and silicate glasses are due to Si-O-Si, Si-O-Al, and/or Al-O-Al [abbreviated as Si-(Al)-O] fundamental vibrational modes (e.g., McMillan 1984; McMillan and Hofmeister 1988). There are several distinct mid-IR bands

related to Si-(Al)-O vibrations in silicate glasses: in particular, asymmetric stretching vibrations contribute to at least five bands between ~700 and ~1250 cm⁻¹ (~8 and ~14.2 μm) (e.g., Bell et al. 1968; Furukawa et al. 1981; McMillan 1984; Dowty 1987; Poe et al. 1992; Parot-Rajaona et al. 1994; Agarwal et al. 1995; McMillan and Wolf 1995; McMillan et al. 1998; King et al. 2004; Dalby and King 2006). The individual bands are difficult to discern in mid-IR spectra of silicate glasses, but instead a "broad peak" is observed in transmission, reflectance, and emission IR that is centered at ~900–1100 cm⁻¹ in silicate glasses. In intermediate-felsic silicate glasses, an additional band/shoulder is observed at ~1150–1230 cm⁻¹. It is well established that the location of the broad peak shifts toward higher wavenumbers (shorter wavelengths) as a function of increasing mol% SiO₂ (or Si/O) in glasses (e.g., Heaton and Moore 1957; Sweet and White 1969; Logan et al. 1975; Efimov 1996; Byrnes et al. 2007; King et al. 2008; Dalby et al. in prep.). The ~1150–1230 cm⁻¹ band also shifts toward higher wavenumbers as a function of increasing mol% SiO₂ (e.g., Dalby et al. 2006; King et al. 2008; Dalby et al. in prep.).

The locations and shapes of the KK abs. peak and its shoulder are a function of the average Si-O force constants, Si-O-Si bond angles and linkages (e.g., Si-O-Si, Si-O-Al, Si-O-Na, etc.) and the relative contributions of each of the structural units to the overall glass structure (e.g., Efimov 1996; Mysen and Richet 2005). Each glass is made up of network formers (e.g., Si⁴⁺, Al³⁺, Ti⁴⁺)

* E-mail: celeste.dufresne@gmail.com

† Current address: Department of Earth Sciences, St. Francis Xavier University, Antigonish, Nova Scotia, Canada.

that polymerize the glass structure, network modifiers (M; e.g., Na⁺, K⁺, Mg²⁺, and Ca²⁺) that break apart the silicate network (e.g., Henderson 2005; Mysen and Richet 2005; Calas et al. 2006) and charge compensators (e.g., Na⁺ and K⁺) that account for trivalent cations acting as network formers (e.g., Al³⁺) (e.g., Neuville and Mysen 1996; Angeli et al. 2000; De Maeyer et al. 2002). The network formers bond to either bridging O atoms that are bound to a network former (e.g., Si-O-Si, Si-O-Al, etc.) or non-bridging O atoms where there is a network modifier (e.g., Si-O-M). Typically, Qⁿ terminology is used to refer to the number of bridging O atoms (n) per network forming atom (Engelhardt and Michel 1987). For example, if a glass has a value of Q⁴ it is highly polymerized with each Si tetrahedrally bonded to four bridging O atoms (e.g., SiO₂ glass). A value of Q⁰ refers to a melt where each Si is bonded to a non-bridging oxygen (e.g., orthosilicate glass).

In the context of the glass structure, the “broad peak” is considered to be related to asymmetric stretches of Q⁴ and Q³ species (e.g., Si-O-Si, Si-O-Al, Si-O-M) (review in King et al. 2004). The ~1150–1230 cm⁻¹ shoulder is related to either asymmetric stretching vibrations of variable angle Si-O-Si bridges (McMillan and Pirou 1982) or asymmetric stretching vibrations of bridging Si-O-Si and non-bridging Si-O-M (Efimov 1996).

Very little work has been done to systematically examine how SiO₂ content affects mid-IR spectra in glasses in multi-component tholeiitic basaltic glasses with a small range in SiO₂ (45 to 55 wt%). Other elements that vary widely in basaltic glasses have not been investigated in detail (e.g., FeO_{total}, Fe³⁺/Fe²⁺, and alkalis). To our knowledge, there are no studies that directly address how FeO_{total} and Fe³⁺/Fe²⁺ affect the broad mid-IR peak in glasses, despite the fact that some authors suggest that Fe³⁺ may substitute in the Si site in glasses because it may act as a network former (e.g., Henderson 2005; Mysen and Richet 2005). Both FeO_{total} and Fe³⁺/Fe²⁺ in silicate glasses affect features in the ultraviolet-visible-near IR region that are attributed to Fe electronic transitions (Bell and Mao 1976; Kakadapu et al. 2003). In addition, there are no systematic studies investigating whether the alkali content of basaltic glasses changes mid-IR spectra. However, it is known that the addition of alkalis causes the spectral shape and location of the broad spectral peak to change. For example, in binary and ternary sodium silicate glasses, as Na₂O increases the broad peak shifts to lower wavenumbers and becomes resolved into two peaks, located at ~920–975 and ~1040–1070 cm⁻¹ (Sweet and White 1969; Domine and Piriou 1983; Merzbacher and White 1988).

This study examines 100 mid-IR spectra of basaltic glasses with different SiO₂, FeO_{total}, Fe³⁺/Fe²⁺, and alkali contents, to better constrain chemical controls on IR spectra in glasses. In the absence of theoretical models to predict the relationships between IR spectra and natural glass compositions, it is necessary to make experimental measurements. Ultimately, this knowledge may be used to create spectral libraries of glass end-members, to improve fitting procedures for IR spectra collected in the laboratory or with remote sensors, and to provide insight into glass structure.

EXPERIMENTAL METHODS

Eighteen basaltic glasses (Table 1) were prepared using 1921 Pu'u O'o tholeiitic basalt from Kilauea, Hawaii (e.g., Holloway and Burnham 1972). The

basalt was ground in agate under ethanol to <30 μm then sintered in a Pt crucible in a box furnace at 1100 °C for 6 h. The grinding-sintering steps were repeated three times before mixing the basalt powder with polyethylene oxide to form a paste (after O'Neill and Mavrogenes 2002). The paste was mounted on loops of Re ribbon (0.025 mm thick by 0.80 mm wide) or Pt or Fe-doped Pt wire (0.25 mm diameter), then hardened at 110 °C for 30 min. The Fe-doped Pt wire was prepared by submersing the Pt wire in the 1921 Kilauea basalt at 1400 °C, for 4–7 h, at an oxygen fugacity (*f*_{O₂}) of three log units below the nickel-nickel oxide buffer, and it was cleaned in Na₂CO₃ (at 1000 °C for ~20 min) followed by HCl.

Basaltic melts were synthesized in the hot spot of a Deltech vertical furnace at 1400 °C for 5 to 200 h (Table 1). To quench the basaltic melt to a glass, an electric current was applied to a thin Pt wire holding the sample loops causing them to fall into a container cooled by ice water. Different *f*_{O₂} conditions in the furnace were created using air or CO₂-CO gases, and *f*_{O₂} was monitored using a zirconia electrode (Table 1). Henceforth, we will refer to log*f*_{O₂} values relative to the nickel-nickel oxide (NNO) buffer curve (e.g., NNO+3 has a log*f*_{O₂} value three log units higher than the NNO buffer curve).

To synthesize basaltic glasses of similar but slightly different compositions, we took advantage of Fe loss (to/from the sample loop) and alkali loss (to air) during experimental synthesis. As expected, glasses synthesized using Fe-doped Pt wire at high *f*_{O₂} had higher FeO_{total} contents than the starting basaltic powders because Fe diffused from the wire to the melt because the Fe-Pt alloy was created at a lower *f*_{O₂} (e.g., Grove 1981). Glasses synthesized using Fe-doped Pt or Pt wire at low *f*_{O₂} had lower FeO_{total} contents than the starting basaltic powder because Fe diffused from the melt to the wire. In contrast, glasses synthesized at a high *f*_{O₂} on Pt wire had similar Fe contents to the starting basaltic powder because Fe³⁺ dominated the melt and does not easily alloy with Pt. Glasses synthesized on Re ribbon had Fe contents similar to the starting material.

To obtain glasses with low alkali contents, we promoted “alkali loss” from the glasses (following Donaldson 1979) by synthesizing them under CO₂ gas for long run durations (100–200 h). Alkali-rich glasses were synthesized by adding Na₂CO₃ or K₂CO₃ to the basalt (Table 1), sintering (at 800 °C) and grinding twice, and melting samples on Pt wire at 1400 °C under a CO₂ gas flow for 5 h.

For analysis, aliquots of glass were mounted in epoxy and polished (to 1 μm). Two other basaltic glasses (DL0413 and B-Alk; Table 1) were synthesized by other lab personnel and were examined to slightly expand the compositional range.

ANALYTICAL METHODS

Electron microprobe analysis

Electron microprobe analyses of the basaltic glasses were performed by Glenn Poirier with a JEOL 733 Superprobe housed at the Canadian Museum of Nature. Wavelength dispersive spectrometry analyses were conducted, using a beam current of 20 nA, a beam diameter of 10 μm, and an accelerating voltage of 15 kV, on at least three locations on each of the individual glass pieces.

Mössbauer spectroscopy

Mössbauer spectroscopy for eight synthetic basaltic glasses (Table 1) was performed at Mount Holyoke College, South Hadley, Massachusetts. Seven glasses were selected because they cover a wide range of *f*_{O₂} values (NNO-3 to NNO+5) and have similar SiO₂ (50.7 ± 0.7 wt%) and FeO_{total} (11.0 ± 0.9 wt%) contents. An additional glass (NNO-3 dPt) was chosen because of its low *f*_{O₂}, but it has different SiO₂ and FeO_{total} (54.9 and 6.9 wt%, respectively). Sample mounts were prepared by gently crushing 15–18 mg of glass under acetone, then mixing with sugar under acetone. Each crushed glass was heaped in a sample holder confined by polyimide tape. Mössbauer spectra were acquired at 295 K using a source of ~50 mCi ⁵⁷Co in Rh on a WEB Research Co. model WT302 spectrometer. For each glass, the fraction of the baseline due to the Compton scattering of 122 keV gammas by electrons inside the detector was determined and subtracted.

Run times were 24–48 h for each spectrum, and baseline counts were ~6–14 million after the Compton correction, as needed to obtain reasonable counting statistics on these very low Fe glasses. Data were collected in 2048 channels, corrected for nonlinearity, and referenced to the spectrum of the 25 μm Fe foil used for calibration. Data were then folded before fitting.

To model the data, we used an in-house program from Eddy De Grave and Toon Van Alboom at the University of Ghent, in Belgium. All the spectra were processed using the Dist3e program, which models spectra using quadrupole splitting or hyperfine field distributions for which the subspectra are constituted by Lorentzian shaped lines. It uses velocity approximations rather than solving

TABLE 1. Experimental and analytical data for the basaltic glass subset and a Fe-free basalt

Glass*	NNO-4 Re	NNO-3 Re	NNO-3 dPt_1	NNO-3 dPt
wt%†				
SiO ₂	51.60 (0.10)	51.13 (0.20)	54.86 (0.57)	53.19 (0.25)
TiO ₂	2.67 (0.01)	2.62 (0.02)	2.79 (0.04)	2.77 (0.06)
Al ₂ O ₃	11.94 (0.04)	11.61 (0.14)	12.50 (0.13)	12.23 (0.15)
FeO _{total}	11.46 (0.07)	11.29 (0.07)	6.91 (0.81)	8.53 (0.19)
MnO	0.17 (0.01)	0.16 (0.01)	0.16 (0.03)	0.15 (0.03)
MgO	9.94 (0.05)	10.01 (0.05)	10.56 (0.12)	10.35 (0.17)
CaO	10.74 (0.02)	10.43 (0.06)	11.21 (0.10)	10.89 (0.13)
Na ₂ O	0.40 (0.01)	0.44 (0.02)	0.66 (0.10)	1.36 (0.03)
K ₂ O	0.25 (0.01)	0.24 (0.01)	0.33 (0.01)	0.40 (0.02)
P ₂ O ₅	0.15 (0.01)	0.15 (0.01)	0.11 (0.01)	0.22 (0.01)
Total	99.3	98.08	100.08	100.08
Mg no.	60.7 (0.2)	61.2 (0.2)	73.1 (2.4)	68.4 (0.8)
Total alkali	0.65 (0.01)	0.68 (0.03)	0.99 (0.11)	1.76 (0.03)
Al/(Al+Si)	0.214 (0.001)	0.211 (0.001)	0.212 (0.001)	0.213 (0.002)
Mössbauer Fe ³⁺ /Fe ²⁺		0.05	0.08	
No. of correlated IR and probe analyses spots	4	4	10	8
T range (°C)	1414–1417	1413–1417	1413–1416	1414–1417
log (f _{O₂})	-10.01	-8.69	-8.7	-8.66
Duration (h)	5	5	5	5
Other				
Wavenumber of max. μ R-IR (cm ⁻¹)†	967 (1)	966 (2)	979 (3)	989 (4)
Wavenumber of KK abs. max. (cm ⁻¹)†	1038 (0)	1040 (3)	1050 (3)	1044 (2)
FWHM of KK abs. peak (cm ⁻¹)†	222 (1)	222 (1)	228 (3)	212 (3)
Glass*	NNO-2 Re	NNO-1.5 Re	NNO-1.5 dPt	NNO+1 Pt
wt%†				
SiO ₂	52.28 (0.17)	51.52 (0.23)	51.42 (0.09)	50.86 (0.13)
TiO ₂	2.65 (0.03)	2.73 (0.01)	2.74 (0.06)	2.71 (0.05)
Al ₂ O ₃	12.00 (0.07)	11.92 (0.09)	12.05 (0.06)	11.85 (0.01)
FeO _{total}	11.59 (0.06)	11.32 (0.11)	10.37 (0.05)	9.67 (0.26)
MnO	0.16 (0.02)	0.16 (0.03)	0.16 (0.05)	0.17 (0.01)
MgO	10.01 (0.04)	9.85 (0.08)	9.88 (0.11)	9.90 (0.03)
CaO	10.76 (0.05)	10.73 (0.08)	10.67 (0.05)	10.60 (0.03)
Na ₂ O	0.33 (0.04)	0.06 (0.01)	1.48 (0.03)	1.80 (0.03)
K ₂ O	0.05 (0.02)	0.03 (0.01)	0.43 (0.03)	0.48 (0.01)
P ₂ O ₅	0.24 (0.01)	0.23 (0.02)	0.21 (0.01)	0.21 (0.01)
Total	100.07	98.54	99.4	98.26
Mg no.	60.6 (0.2)	60.8 (0.4)	62.9 (0.3)	64.6 (0.6)
Total alkali	0.39 (0.06)	0.08 (0.01)	1.91 (0.04)	2.28 (0.02)
Al/(Al+Si)	0.213 (0.001)	0.214 (0.002)	0.216 (0.001)	0.215 (0.000)
Mössbauer Fe ³⁺ /Fe ²⁺		0.1	0.08	0.54
No. of correlated IR and probe analyses spots	5	4	5	3
T range (°C)	1414–1418	1414–1420	1413–1416	1414–1417
log (f _{O₂})	-7.63	-7.11	-7.12	-4.55
Duration (h)	5	5	5	5
Other				
Wavenumber of max. μ R-IR (cm ⁻¹)†	965 (2)	960 (3)	988 (2)	991 (1)
Wavenumber of KK abs. max. (cm ⁻¹)†	1039 (1)	1039 (2)	1040 (1)	1040 (2)
FWHM of KK abs. peak (cm ⁻¹)†	227 (1)	234 (1)	204 (1)	201 (1)
Glass*	NNO+3 Pt	NNO+3 dPt	Alk-5A	Alk-5B
wt%†				
SiO ₂	50.25 (0.45)	49.70 (0.61)	50.90 (0.39)	50.02 (0.09)
TiO ₂	2.60 (0.04)	2.59 (0.03)	2.67 (0.02)	2.65 (0.08)
Al ₂ O ₃	11.68 (0.12)	11.95 (0.370)	11.78 (0.09)	11.59 (0.05)
FeO _{total}	10.78 (0.17)	12.65 (0.24)	10.19 (0.17)	10.61 (0.09)
MnO	0.15 (0.03)	0.16 (0.02)	0.17 (0.03)	0.16 (0.03)
MgO	9.68 (0.07)	9.59 (0.16)	9.64 (0.15)	9.52 (0.10)
CaO	10.49 (0.05)	10.24 (0.08)	10.42 (0.100)	10.41 (0.03)
Na ₂ O	1.94 (0.03)	1.89 (0.06)	2.57 (0.08)	3.04 (0.06)
K ₂ O	0.48 (0.02)	0.45 (0.02)	0.49 (0.01)	0.47 (0.01)
P ₂ O ₅	0.22 (0.01)	0.18 (0.04)	0.15 (0.03)	0.19 (0.02)
Total	98.26	99.39	98.98	98.65
Mg no.	61.6 (0.5)	57.5 (0.8)	62.8 (0.1)	61.5 (0.4)
Total alkali	2.42 (0.03)	2.34 (0.07)	3.06 (0.09)	3.51 (0.06)
Al/(Al+Si)	0.215 (0.001)	0.221 (0.007)	0.214 (0.000)	0.215 (0.001)
Mössbauer Fe ³⁺ /Fe ²⁺	1.13	1.02		
No. of correlated IR and probe analyses spots	6	10	4	5
T range (°C)	1414–1418	1408–1412	1414–1417	1414–1417
log (f _{O₂})	-2.95	-2.95	-2.95	-2.95
Duration (h)	5	5	5	5
Other			1.3% Na ₂ CO ₃	2.2% Na ₂ CO ₃
Wavenumber of max. μ R-IR (cm ⁻¹)†	991 (1)	978 (4)	997 (1)	997 (1)
Wavenumber of KK abs. max. (cm ⁻¹)†	1040 (1)	1036 (1)	1040 (2)	1039 (1)
FWHM of KK abs. peak (cm ⁻¹)†	200 (1)	203 (2)	194 (1)	189 (1)

Continued on next page

TABLE 1.—CONTINUED

Glass*	Alk-5C	Alk-5D	Alk-100	Alk-200	
wt%†					
SiO ₂	51.62 (0.24)	51.05 (0.37)	51.70 (0.05)	52.79 (0.47)	
TiO ₂	2.61 (0.05)	2.61 (0.01)	2.71 (0.04)	2.77 (0.04)	
Al ₂ O ₃	11.75 (0.14)	11.66 (0.08)	12.02 (0.21)	12.22 (0.21)	
Fe _{total}	10.78 (0.02)	10.53 (0.15)	10.73 (0.08)	10.31 (0.16)	
MnO	0.16 (0.01)	0.15 (0.03)	0.17 (0.03)	0.16 (0.02)	
MgO	9.78 (0.11)	9.68 (0.14)	10.02 (0.13)	10.17 (0.17)	
CaO	10.32 (0.07)	10.32 (0.10)	10.67 (0.13)	10.69 (0.05)	
Na ₂ O	1.98 (0.03)	1.89 (0.03)	1.43 (0.04)	0.87 (0.03)	
K ₂ O	0.95 (0.02)	1.71 (0.06)	0.44 (0.02)	0.38 (0.01)	
P ₂ O ₅	0.20 (0.03)	0.17 (0.02)	0.07 (0.00)	0.04 (0.01)	
Total	100.12	99.75	99.97	100.41	
Mg no.	61.8 (0.3)	62.1 (0.5)	62.5 (0.4)	63.8 (0.4)	
Total alkali	2.92 (0.04)	3.60 (0.07)	1.87 (0.05)	1.25 (0.03)	
Al/(Al+Si)	0.211 (0.002)	0.212 (0.000)	0.215 (0.001)	0.214 (0.001)	
Mössbauer Fe ³⁺ /Fe ²⁺					
No. of correlated IR and probe analyses spots	4	5	4	3	
T range (°C)	1408–1412	1408–1412	1408–1412	1408–1412	
log (f _{o₂})	-2.95	-2.95	-2.95	-2.95	
Duration (h)	5	5	100	200	
Other	1.4% K ₂ CO ₃	2.8% K ₂ CO ₃			
Wavenumber of max. μ R-IR (cm ⁻¹)†	993 (1)	1001 (1)	980 (1)	972 (1)	
Wavenumber of KK abs. max. (cm ⁻¹)†	1041 (1)	1041 (1)	1041 (1)	1044 (3)	
FWHM of KK abs. peak (cm ⁻¹)†	199 (1)	189 (1)	211 (1)	223 (1)	
Glass*	NNO+5 Pt	NNO+5 dPt	DL0413	B-Alk‡	Fe-Free MORB
wt%†					
SiO ₂	50.19 (0.15)	48.87 (1.17)	50.87 (0.32)	48.25	59.20 (0.28)
TiO ₂	2.65 (0.05)	2.54 (0.07)	2.59 (0.08)	4.22	1.29 (0.04)
Al ₂ O ₃	11.69 (0.07)	11.30 (0.32)	12.13 (0.14)	12.38	18.27 (0.62)
Fe _{total}	10.97 (0.06)	14.39 (1.77)	10.36 (0.16)	14.51	0.12 (0.05)
MnO	0.17 (0.02)	0.16 (0.04)	0.16 (0.06)	0.22	
MgO	9.74 (0.10)	9.45 (0.27)	9.37 (0.24)	5.35	11.14 (0.13)
CaO	10.39 (0.06)	10.07 (0.16)	10.51 (0.14)	10	7.55 (0.16)
Na ₂ O	1.86 (0.04)	1.68 (0.10)	2.06 (0.06)	2.97	1.73 (0.16)
K ₂ O	0.49 (0.02)	0.39 (0.03)	0.48 (0.03)	0.77	0.04 (0.01)
P ₂ O ₅	0.22 (0.02)	0.19 (0.01)	0.28 (0.04)	0.56	0.03 (0.02)
Total	98.36	99.05	98.81	99.23	99.37
Mg no.	61.3 (0.3)	53.9 (3.7)	61.7	39.7	
Total alkali	2.35 (0.06)	2.06 (0.13)	2.54 (0.09)	3.74	1.78 (0.15)
Al/(Al+Si)	0.215 (0.001)	0.214 (0.002)	0.219	0.232	0.267
Mössbauer Fe ³⁺ /Fe ²⁺	1.17				
No. of correlated IR and probe analyses spots	4	10	1§	1§	1§
T range (°C)	1413–1417	1408–1412	1300		1400
log (f _{o₂})	-0.68	-0.68	NNO-2	air	air
Duration (h)	5	5	3	N/A	2
Other			P = 0.5 GPa; 0.97 wt% H ₂ O		
Wavenumber of max. μ R-IR (cm ⁻¹)†	987 (2)	969 (6)			
Wavenumber of KK abs. max. (cm ⁻¹)†	1040 (1)	1038 (4)	1037.5	1033.7	1080 (3)
FWHM of KK abs. peak (cm ⁻¹)†	206 (1)	209 (2)	193	195	244 (7)

* The sample name gives the logf_{o₂} conditions relative to the NNO buffer, the loop type used during the synthesis (Re, Pt, or Fe-doped Pt wires) and, where appropriate, the name of the glass bead.

† wt% and spectral parameters are reported as "value (error)".

‡ The bulk chemistry for B-Alk was taken from Oskarsson et al. (1982).

§ Electron microprobe and IR data obtained from an average of multiple analyses, not correlated spot analyses.

the full Hamiltonian. This program does not presume any particular shape of the distribution. Widths (Γ), isomer shifts (δ), and quadrupole splittings (Δ) of the doublets were allowed to vary during fitting. If the widths fell below 0.24 mm/s, they were held constant. Overall errors on isomer shift and quadrupole splitting are ± 0.05 –0.1 mm/s, but errors on total Fe³⁺ areas are probably ± 1 –3% absolute.

It is especially important to note that some aspects of the fits (notably, the distribution of Fe²⁺ among sites) to the Mössbauer spectra are somewhat non-unique. In most silicate glasses, Fe²⁺ and Fe³⁺ occupy a large array of different geometries and sizes of coordination polyhedra. For this reason, there are no sharp, well-resolved doublets corresponding to particular sites (as in crystalline materials). Rather, there is a continuum of site types, which could be represented by a continuum of doublets. For this reason, we fit the spectra with distributions, and the choice of number of distributions for Fe²⁺ and Fe³⁺ relied on simplicity: we report here the minimum number of distributions for each cation that were necessary to model the data with a χ^2 value <3. Thus, the apportionment of areas among Fe²⁺ peaks is probably non-unique; in other words, the areas reported in Table 2 for different sub-distributions of Fe²⁺ are likely to be highly model-dependent, and reflect only ranges of coordination types. However, repeated fits to these spectra demonstrated

a typical result for glass fits: the number of Fe²⁺ distributions does not affect the percentage of Fe in the Fe³⁺ doublet. For this reason, the errors on total Fe³⁺ are as stated above, but the errors on distribution of area among Fe²⁺ doublets are probably ± 10 –30% absolute.

Micro-reflectance Fourier Transform infrared spectroscopy

Micro-reflectance Fourier Transform infrared (μ R-FTIR) analyses of the basaltic glasses were collected using a Nicolet FTIR spectrometer with a micro-scope attachment in the Experimental Analysis Laboratory at the University of Western Ontario. Specifically we used a Nexus 670 spectrometer with a Globar source, XT-KBr beamsplitter, and a Continuum microscope with a MCT/A detector that was purged with dry air. Each spectrum was collected in a spectral range of 5400–650 cm⁻¹, over 300 scans, with 4 cm⁻¹ resolution, in a 100 \times 100 μ m sampling area. A background spectrum, collected on a gold slide was divided from the glass spectrum. Spectra were obtained for each glass in approximately the same locations in which the electron microprobe analyses were conducted. The raw spectra

TABLE 2. Mössbauer parameters (isomer shifts = δ , quadrupole splittings = Δ , and widths = Γ)

Glass		NNO-3 Re	NNO-3 dPt	NNO-1.5 Re	NNO-1.5 dPt	NNO+1 Pt	NNO+3 Pt	NNO+3 dPt_1	NNO+5 Pt
^{IV} Fe ²⁺	δ (mm/s)	1	0.99	0.98	0.98	0.99	0.96	0.9	0.92
	Δ (mm/s)	1.54	1.57	1.57	1.55	1.56	1.55	1.56	1.56
	Γ (mm/s)	0.58	0.59	0.64	0.64	0.46	0.39	0.47	0.39
	Area(%)	46	48	47	46	27	15	14	11
^{IV} Fe ²⁺	δ (mm/s)	1.06	1.07	1.07	1.06	1.02	0.96	0.92	0.92
	Δ (mm/s)	1.94	2	2.11	1.9	2.02	2.1	2.11	2.13
	Γ (mm/s)	0.3	0.3	0.3	0.3	0.3	0.3	0.3	0.3
	Area(%)	34	36	36	33	26	23.2	23	19.2
^{IV} Fe ²⁺	δ (mm/s)	1.09	1.1	1.09	1.11	1.07	0.93	0.93	0.9
	Δ (mm/s)	2.57	2.67	2.63	2.57	2.56	2.87	2.71	2.73
	Γ (mm/s)	0.3	0.3	0.3	0.3	0.3	0.3	0.3	0.4
	Area(%)	15	9	9	14	12	9	13	16
^{VI} Fe ³⁺	δ (mm/s)	0.17	0.15	0.15	0.1	0.38	0.42	0.49	0.47
	Δ (mm/s)	0.42	0.48	0.5	0.58	1.01	1.01	0.95	0.96
	Γ (mm/s)	0.3	0.3	0.3	0.3	0.88	0.69	0.69	0.73
	Area(%)	5	7	9	7	35	53	51	54
	χ^2	2.61	1.61	1.61	2.05	1.38	1.39	1.34	1.49
	Fe ³⁺ /Fe ²⁺	0.053	0.075	0.075	0.099	0.539	1.02	1.128	1.174

were collected in units of percent reflectance (%R) and the peak maxima were determined using OMNIC version 6.1 software.

To facilitate accurate comparisons of our glass spectra, we transformed each spectrum from reflectance units into absorbance units using a Kramers-Kronig (KK) transform (e.g., Sweet and White 1969; McMillan and Hofmeister 1988). We use the term "KK abs. peak" to refer to the peak produced by the KK transform of the broad spectral feature that is related to Si-(Al)-O vibrational modes.

The KK transformation allows accurate comparisons of spectra of different glass compositions because it removes the effects of the optical constants (McMillan and Hofmeister 1988). Specifically, the KK transformation removes the effects of the refractive index, n , and the dielectric constant, ϵ , that vary as a function of wavelength in a specular reflectance spectrum. The refractive index of a medium, n , is defined by

$$n = c/v \quad (1)$$

where c is the speed of light in a vacuum and v is the velocity of light as it passes through the medium. The refractive index is related to the dielectric constant, ϵ , by

$$\epsilon = n^2 \quad (2)$$

In a reflectance spectrum, the refractive index and dielectric constant are comprised of a real and an imaginary portion, which are related as follows:

$$n = n' + in'' \quad (3)$$

$$\epsilon = n'^2 - n''^2 + 2in'n'' \quad (4)$$

where n' is the real portion of the refractive index, i is $\sqrt{-1}$, and n'' is the imaginary portion of the refractive index. These terms are related to a reflectance spectrum by

$$R = \frac{(n'-1)^2 + (n'')^2}{(n'+1)^2 + (n'')^2} \quad (5)$$

where R is the infrared reflection coefficient. The real and imaginary parts of this equation are related to each other through:

$$r_i = r e^{i\theta} \quad (6)$$

where r_i is the imaginary part of the reflectivity (\sqrt{R}), r is the real part of the reflectivity, and θ is the phase shift, which is proportional to the magnitude of the absorption coefficient. A KK transformation is performed to determine the phase shift and produce an absorption spectrum. The formula for the KK transformation is

$$\theta(v_i) = \frac{2v_i}{\pi} \int_0^\infty \frac{\ln r(v) - \ln r(v_i)}{v_i^2 - v^2} dv \quad (7)$$

where v is the real portion of the frequency and v_i is imaginary portion of the frequency.

Because the KK transformation must be evaluated over a range of wavelengths ranging from zero to infinity, the wings of each reflectance spectrum are extrapolated in the Nicolet OMNIC v. 6.1 software. To ensure uniform extrapolation, we sampled a constant wavenumber range (5400–650 cm^{-1}). Spectra were smoothed over a 40.5 cm^{-1} window (e.g., Moore et al. 2000) before the KK transform. The baselines for both raw reflectance and KK absorbance spectra were relatively flat; thus, the baseline correction, which was performed after the KK transform, changed the KK abs. peak locations by less than 0.5 cm^{-1} (well within the error of the measurement). The peak locations were determined using OMNIC version 6.1 software. Full-width at half maximum (FWHM) values were determined by finding the difference in wavenumber between the points located half way between the baseline and the peak maximum in each spectrum.

RESULTS

Glass composition

Electron microprobe data for the synthetic basaltic glasses (Table 1) indicate that each glass is crystal-free and homogeneous within error. As intended, the collection of glasses displays a compositional range from basalt to basaltic andesite (Le Maitre et al. 2002). The range in composition is due to iron and alkali loss, minor differences in the synthesis conditions for each sample (e.g., sample-to-loop volumes, surface area/volume, temperatures) and possible variation in our starting material. Importantly, there is negligible compositional variation within an individual glass (Appendix Table 1¹). We report average analyses in Table 1, but individual analysis locations (Appendix Table 1¹) were considered when comparing IR spectra to compositions.

Electron microprobe data revealed that the synthetic basaltic glasses, excluding the Fe-free basalt (Table 1), have similar compositions for all oxides except SiO_2 (47.18–55.57 wt%), $\text{FeO}_{\text{total}}$ (6.06–16.30 wt%), Na_2O (0.04–3.12 wt%), and K_2O (0.02–1.80 wt%) (Appendix Table 1). Although Al-O or Si-Al-O vibrations likely contribute to the KK abs. peak, we will not discuss Al further because it is relatively constant in our data set [$\text{Al}_2\text{O}_3 = 11.89 \pm 0.37$ wt%; $\text{Al}/(\text{Al}+\text{Si}) = 0.209\text{--}0.232$].

¹ Deposit item AM-09-050, Appendix Table 1 and Appendix Figures 1 and 2. Deposit items are available two ways: For a paper copy contact the Business Office of the Mineralogical Society of America (see inside front cover of recent issue) for price information. For an electronic copy visit the MSA web site at <http://www.minsocam.org>, go to the American Mineralogist Contents, find the table of contents for the specific volume/issue wanted, and then click on the deposit link there.

All of the basaltic glasses contain CIPW normative plagioclase, diopside, hypersthene, quartz, and orthoclase with accessory ilmenite, magnetite, hematite, and apatite (Appendix Table 1¹) and plot as tholeiitic on a basalt tetrahedron (Yoder and Tilley 1962). Four glasses are classified as basaltic andesites (Le Maitre et al. 2002; NNO-3 dPt_1, NNO-3 dPt, NNO-2 Re, Alk-200; Appendix Table 1); nonetheless all glasses will be considered when interpreting data.

Mössbauer $\text{Fe}^{3+}/\text{Fe}^{2+}$ values

Measured $\text{Fe}^{3+}/\text{Fe}^{2+}$ values were determined from Mössbauer spectroscopy using the parameters given in Table 2. Three representative spectral fits are shown in Figure 1. The eight basaltic glasses that were examined using Mössbauer spectroscopy have measured $\text{Fe}^{3+}/\text{Fe}^{2+}$ from 0.05 to 1.17. Measured $\text{Fe}^{3+}/\text{Fe}^{2+}$ systematically increases as the synthesis f_{O_2} increases [$\text{Fe}^{3+}/\text{Fe}^{2+} = 0.18x + 0.48$, where $x = \log f_{\text{O}_2}$ relative to NNO, $R^2 = 0.94$] for all but the most oxidized sample (NNO+5) that likely did not equilibrate in the experimental time frame. Nonetheless, for the purpose of examining the role of $\text{Fe}^{3+}/\text{Fe}^{2+}$ on IR spectral features, it is only important that $\text{Fe}^{3+}/\text{Fe}^{2+}$ is known.

Micro-reflectance FTIR spectra

Approximately the same location in each synthetic glass chip was examined using the electron microprobe (10 μm diameter) and μR -FTIR analyses (100 \times 100 μm). The difference in spot

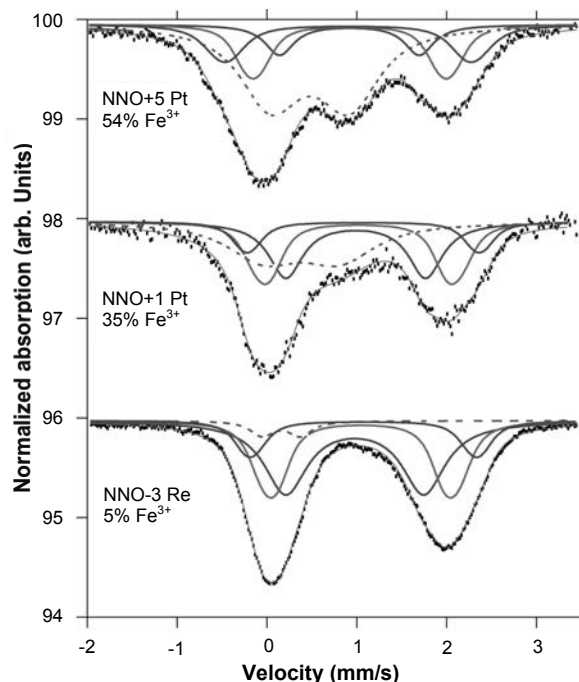


FIGURE 1. Mössbauer spectra for three basaltic glasses synthesized at NNO+5 to NNO-3 (NNO+5 Pt, NNO+1 Pt, and NNO-3 Re). Individual Mössbauer data points are shown as vertical lines scaled to represent standard error. The sum of peaks fitted to each spectrum is shown as a thin black line passing through the Mössbauer data points. Individual distributions are shown as pairs of doublets, where thicker solid doublets represent Fe^{2+} and the dashed doublets represent Fe^{3+} .

size is negligible because the average chemistry for individual glass pieces indicates that the glass pieces are homogeneous within microprobe error.

Figure 2a shows μR -FTIR spectra for two glasses synthesized at NNO+3 whose SiO_2 contents in the very same area of the sample (see Appendix Table 1¹) are 53.33 and 48.57 wt% and alkali contents are 1.27 and 2.28 wt%. (Alk-200 and NNO+3 dPt). The two spectra are very similar and show the characteristic spectral shape of all spectra collected in this study: a slight shift to higher wavenumbers (likely due to Fe electronic transitions in the visible-near-IR) and a distinct broad peak related to Si-(Al)-O vibrations (as discussed above). For the entire data set of synthetic basaltic glasses, the broad peaks are located from 956 to 1002 cm^{-1} (Appendix Table 1¹). We note that atmospheric and dissolved H_2O and

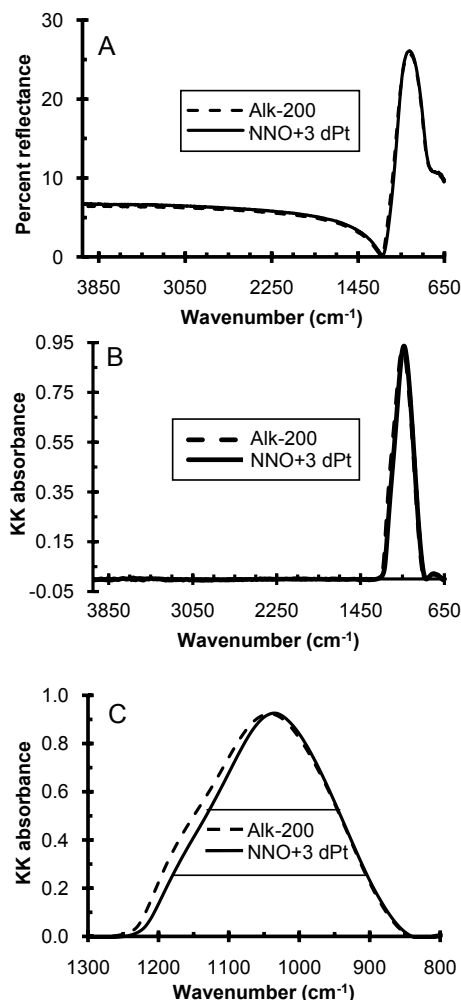


FIGURE 2. Spectra for two representative synthetic basaltic glasses (Alk-200 = dashed; NNO+3 dPt = solid). These glasses were both synthesized at NNO+3, but have different SiO_2 contents (53.33 and 48.57 wt%, respectively) and total alkali contents (1.27 and 2.28 wt%, respectively). (a) Micro-reflectance FTIR spectra for Alk-200 and NNO+3_dPt with peak locations at 972 and 975 cm^{-1} , respectively; (b) KK abs. spectra for Alk-200 and NNO+3_dPt with peak locations at 1042 and 1035 cm^{-1} , respectively; and (c) close-up of KK abs. spectra for Alk-200 and NNO+3_dPt with peak locations at 1042 and 1035 cm^{-1} and FWHM 223 and 205 cm^{-1} , respectively.

CO₂ (~3550 cm⁻¹ and doublet near 2350 cm⁻¹, respectively; Fig. 2a) are below detection in all of the spectra we examined.

Kramers-Kronig absorbance spectra

Figures 2b and 2c show the KK abs. spectra of the same glasses shown in Figure 2a (Alk-200 and NNO+3 dPt). The KK abs. peak is similar overall for these two samples, but the peak location and full-width half maximum (FWHM) exhibit differences that are reported in more detail below (Fig. 2c). Here, we use the term FWHM, but we recognize that is not strictly correct because the KK abs. peak is comprised of a collection of different bands that are specific to different IR-active Si-O vibrational modes (e.g., Dalby and King 2006); however, we use the term FWHM for want of a better term. For the entire data set, the KK abs. peak locations are between 1031 and 1054 cm⁻¹ (Appendix Table 1¹), and the FWHM of the KK abs. peaks range from 188 to 235 cm⁻¹ (Appendix Table 1¹).

Role of composition on the KK abs. peak location and FWHM

Role of SiO₂ and other major element oxides. The location of the KK abs. peak shifts to higher wavenumbers as SiO₂ increases in the basaltic glasses (Fig. 3). This shift occurs in a near-linear manner with KK abs. peak location = 2x + 938 where x = SiO₂ wt% ($R^2 = 0.70$; Fig. 3). The positive correlation between KK abs. peak location and SiO₂ content was expected based on previous work (above).

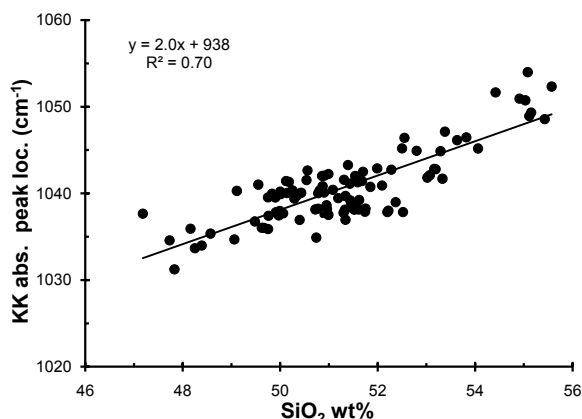


FIGURE 3. KK abs. peak location vs. SiO₂ wt% for 100 correlated spot analyses measured on 20 basaltic glass beads. Wavenumbers have an error of ± 2 cm⁻¹.

TABLE 3. Correlation matrix with R^2 values between the chemical and IR data for (A) 100 correlated spot analyses measured on 20 basaltic glass beads; and (B) 100 correlated spot analyses measured on 20 basaltic glass beads, plus 11 analyses of non-basaltic glasses (King et al. 2008) and analysis of an Fe-free basaltic glass from the extended data set (see text)

(A) 100 correlated spot analyses measured on 20 basaltic glass beads				(B) 100 correlated spot analyses measured on 20 basaltic glass beads, plus 11 analyses of non-basaltic glasses (King et al. 2008) and analysis of an Fe-free basaltic glass from the extended data set			
	KK abs. peak max. (cm ⁻¹)	KK abs. FWHM (cm ⁻¹)	SiO ₂ wt%		KK abs. peak max. (cm ⁻¹)	KK abs. FWHM (cm ⁻¹)	SiO ₂ wt%
SiO ₂ wt%	0.70	0.33		SiO ₂ wt%	0.89	0.21	
FeO wt%	[0.71]	0.07	0.78	FeO wt%	[0.72]	0.13	0.75
MgO wt%	0.38	0.22	0.50	MgO wt%	[0.59]	0.37	0.65
CaO wt%	[0.59]	0.37	0.83	CaO wt%	[0.53]	0.50	0.69
Na ₂ O wt%	0.11	0.86	0.30	Na ₂ O wt%	0.20	0.42	0.26
K ₂ O wt%	0.00	0.44	0.02	K ₂ O wt%	0.11	0.45	0.16
Total alkali wt%	0.06	0.92	0.24	Total alkali wt%	0.22	0.62	0.31

Notes: Data that show significant correlations are shown in bold. Data that show misleading correlations with IR peak maxima, due to a strong relationship with SiO₂ content, are shown in square brackets.

Table 3a shows the linear regression values (R^2) between the KK abs. peak location and compositional variables in the glasses. A high R^2 is reported between the KK abs. peak location and both FeO_{total} ($R^2 = 0.71$) and CaO ($R^2 = 0.59$) (Table 3a). However, we suggest that these relationships are misleading because SiO₂ content is strongly correlated with FeO_{total} ($R^2 = 0.78$) and CaO ($R^2 = 0.83$) (Table 3a). Examination of graphs of the KK abs. peak location vs. either FeO_{total} or CaO, with the data grouped by SiO₂ content, support this claim (Appendix Figure 1 and Appendix Figure 2, respectively¹). Therefore, SiO₂ exerts the major control on the KK abs. peak location in basaltic glasses (Fig. 3 and Table 3a).

Role of Fe³⁺/Fe²⁺. To determine if Fe³⁺/Fe²⁺ affects the ~KK abs. peak location, we grouped the data by SiO₂ content to minimize the effect of SiO₂ content (shown in Fig. 4). Four samples with Fe³⁺/Fe²⁺ values from 0.05–0.54 and 50.86–51.52 wt% SiO₂ have KK abs. peak locations within error of each other. Two samples with Fe³⁺/Fe²⁺ values from 1.13–1.17 and 50.19–50.25 wt% SiO₂ are within error of each other. A final sample with Fe³⁺/Fe²⁺ = 1.02 and a lower SiO₂ content (49.7 wt%) has a KK abs. peak location

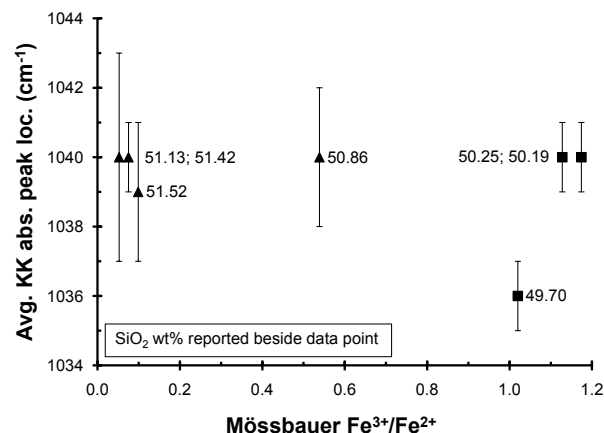


FIGURE 4. Average KK abs. peak location vs. measured Mössbauer Fe³⁺/Fe²⁺ for basaltic glasses with average SiO₂ = 49.7–51.5 wt%. The average SiO₂ content for each glass is given by the numbers next to the symbols. Glass NNO-3 dPt_1 was not included in the plot because it has a SiO₂ content (54.86 wt%, Table 1) well outside of the range of the other glasses and therefore the KK abs. peak location would be expected to be higher. The average KK abs. peak location on multiple locations within a glass is used because the Mössbauer data were collected on a relatively large volume of glass.

that is 4 cm^{-1} lower than the other six samples; consistent with our results that SiO_2 is the major control on the KK abs. peak location. In summary, six of the samples with different $\text{Fe}^{3+}/\text{Fe}^{2+}$ values, but similar SiO_2 contents (50.19–51.52 wt%) have KK abs. peak locations within error, indicating that $\text{Fe}^{3+}/\text{Fe}^{2+}$ does not affect the KK abs. peak location.

Role of alkali elements. Figure 5 shows the spectra of two glasses with similar compositions (SiO_2 , FeO , and CaO), but different alkali contents. The KK abs. peak locations of the two glasses are similar, but the glass with the lower alkali content has a larger FWHM. The larger FWHM is related to an addition of a shoulder (band) at ~ 1150 – 1230 cm^{-1} . This shoulder becomes a more prominent band in felsic compositions (discussed below). However, in most of the basaltic glasses, it is difficult to resolve the shoulder, therefore, we will continue referring to the measurable feature: FWHM.

The entire data set for the basaltic glasses shows that FWHM is negatively correlated with Na_2O and total alkali content (Table 3a; Fig. 6). The observed relationship corresponds to an equation of $\text{FWHM} = -13x + 235$ ($R^2 = 0.92$) where $x = \text{alkali wt}\%$.

DISCUSSION

The role of glass composition on IR spectral features

This study provides, for the first time, a suite of tholeiitic basalt glasses that have been examined for their micro-scale chemistry and mid-IR spectra. Our results show that the KK abs. peak shifts to higher wavenumber as the SiO_2 content increases in basaltic glasses with a small range of SiO_2 contents (Fig. 3). To determine if the correlations observed between the KK abs. peak and composition of basaltic glasses are applicable to a broader compositional range of silicate glasses, we investigated our results in the context of 11 non-basaltic glasses (King et al. 2008; Dalby et al. in prep.), a Fe-free basalt (Table 1), and four Na_2O - SiO_2 glasses (Sweet and White 1969). The non-basaltic glasses ($\text{SiO}_2 = 55.16$ – $80.17 \text{ wt}\%$) include calc-alkaline rhyolites through basalts, phonolites and quartzofeldspathic glasses (King et al. 2008; Dalby et al. in prep.). Our so-called “extended data set of glasses” includes our 100 data points obtained on 20 basaltic glasses (Appendix Table 1¹) plus the data that were available from these additional 16 glasses.

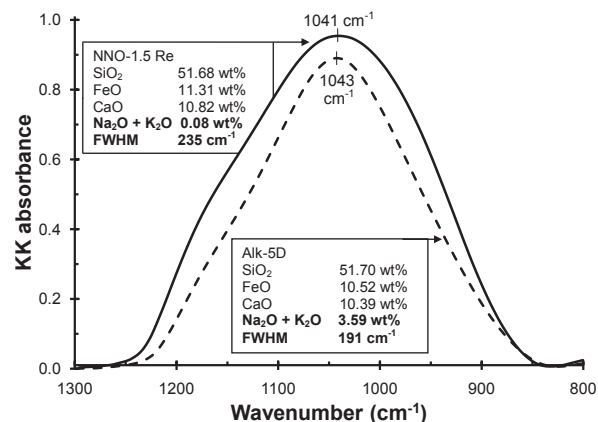


FIGURE 5. KK abs. spectra of basaltic glasses with similar compositions (SiO_2 , $\text{FeO}_{\text{total}}$, and CaO) and peak locations, but with different alkali contents. Wavenumbers have an error of $\pm 2 \text{ cm}^{-1}$.

Role of SiO_2 and other major element oxides. Relationships between the KK abs. peak location and other variables were examined using the extended data set. For the extended data set, the KK abs. peak location is most strongly correlated with SiO_2 content ($R^2 = 0.86$; Fig. 7 and Table 3b; King et al. 2008; Dalby et al. in prep.), as was observed for the glasses of basaltic compositions (Fig. 3). High R^2 values were obtained for linear regressions between the KK abs. peak location with FeO , MgO , and CaO (Table 3b). However, these correlations are considered misleading and are simply a function of the SiO_2 content (as for the basaltic compositions).

We were not able to evaluate the role of $\text{Fe}^{3+}/\text{Fe}^{2+}$ on the KK abs. peak location in the extended data set because the non-basaltic glasses do not have measured $\text{Fe}^{3+}/\text{Fe}^{2+}$. Our extended data set did not lend itself to a systematic examination of the effect of varying the Al content of the glasses. We predict that addition of Al would decrease the wavenumber of the KK abs. peak due to decreasing Si/O in the silicate network (e.g., review in Mysen and Richet 2005), and such an effect is supported by the results of Byrnes et al. (2007).

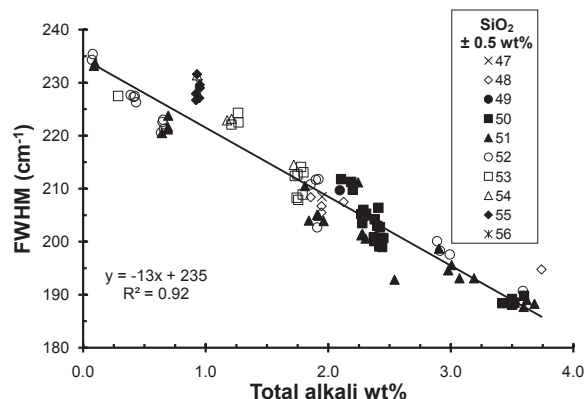


FIGURE 6. The FWHM of the KK abs. peak vs. alkali content of basaltic glasses. Data plotted are for 100 correlated spot analyses measured on 20 basaltic glass beads (Appendix¹) and symbols represent SiO_2 increments. Wavenumbers have an error of $\pm 2 \text{ cm}^{-1}$.

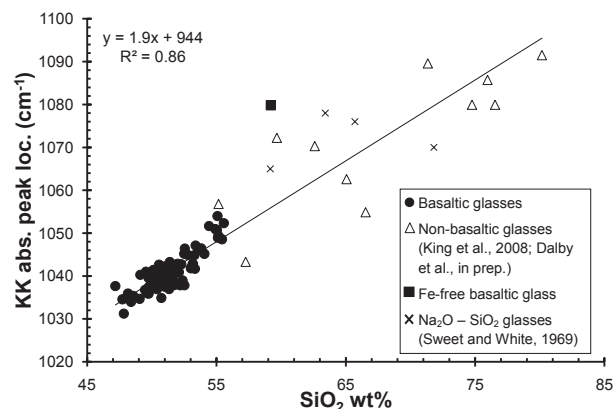


FIGURE 7. The KK abs. peak location vs. SiO_2 content (wt%) for 100 correlated spot analyses measured on 20 basaltic glass beads (closed circles), 11 non-basaltic glasses (King et al. 2008; Dalby et al. in prep.; open triangles), an Fe-free basalt (Table 1; closed square), and four Na_2O - SiO_2 glasses (Sweet and White 1969; crosses) from the extended data set. Wavenumbers have an error of $\pm 2 \text{ cm}^{-1}$.

Role of alkali elements. The glasses in the extended data set did not show a correlation between the FWHM of the KK abs. peak and the alkali content (Table 3b); in contrast to the basaltic glass data subset where there was a strong negative correlation (Figs. 5 and 6; Table 3a). To explain this difference in results we must first examine the influence of glass structure on IR features and, specifically, the role of Na in the melt as a network modifier or charge compensator (see below).

The role of glass structure on IR spectral features on the location and FWHM of the KK abs. peak

Role of SiO₂ on the location of the KK abs. peak. The observation that the IR peak location increases as SiO₂ increases is well known (see introduction) but most studies have focused on simple glass compositions with less than five components (e.g., Sweet and White 1969; Domine and Piriou 1983; Poe et al. 1992; McMillan et al. 1998; Angeli et al. 2000; De Maeyer et al. 2002). Overall, these studies on simple glasses have attributed the increase in the IR peak location with increasing SiO₂ to a decrease in the average bond angle of the dominantly Q⁴ and Q³ species in the bulk glass.

There are few studies on the role of melt structure in complex multi-component silicate compositions, like basalt. However, recent molecular dynamic (MD) models indicate that as SiO₂ content increases in natural silicate glass compositions, the average Qⁿ increases because there are more network formers around Si (Guillot and Sator 2007). Tholeiitic (mid-ocean) basalt glasses are modeled to have an average of ~3 network formers around Si (average ~Q³; although a range of Q species are present), whereas rhyolites have ~4 network formers around Si (average ~Q⁴) (Guillot and Sator 2007). Those authors suggest that Qⁿ increases in a near-linear manner from ultramafic to felsic glasses. Importantly, their model (and other models; e.g., Zotov and Keppler 1998) show that with increasing SiO₂ content, the average bond distance of the glass becomes shorter. The bond distance decreases because there is an increase in the number of higher Qⁿ (more polymerized) Si-O bonds and those bonds have a shorter bond distance than lower Qⁿ (less polymerized) Si-O bonds with less network formers around Si.

Role of Fe³⁺/Fe²⁺ on the KK abs. peak location and FWHM. Despite our finding that Fe³⁺/Fe²⁺ did not affect the basaltic KK abs. peak, we investigated this variable because it has been documented to influence Si-O-Si bond angles in silicate melts (e.g., Bingham et al. 2002). Specifically, Fe³⁺ is considered to be dominantly a fourfold coordination network former in melts (Guillot and Sator 2007; Mysen 2006 and references therein), and would therefore compete with Si in bonding. We suggest that our results do not rule out significant roles for Fe³⁺ as a network former in melts. Instead, we suspect that our compositions had insufficient mole fraction of Fe³⁺ (1.82–5.23 mol%) relative to the mole fraction of Si (18.09–19.86 mol%) to observe any effect on the KK abs. peak. Also, we may not have detected any changes in the IR spectra because the bond distance for Fe³⁺-O is not significantly different than the bond distance for Fe²⁺-O; for example, in basaltic melts these bonds differ by <15% relative to each other (1.82–1.84 and 2.07–2.08 Å, respectively; Guillot and Sator 2007) and similar coordination numbers (4 and 5, respectively; Guillot and Sator 2007).

Role of alkalis on the FWHM of the KK abs. peak. Several studies have documented an increase in the IR broad peak location as alkali cations decrease in a glass (Heaton and Moore 1957; Sweet and White 1969; Efimov 1996). However, most of those studies were undertaken on binary SiO₂-alkali glasses where SiO₂ increased concomitantly with alkali decrease. Our data show no correlation between alkali content and KK abs. peak position (Tables 3a and 3b).

Instead, our data for the basaltic compositions show that the KK abs. peak FWHM decreases as alkalis are added (for samples with and without constant SiO₂ content), but this relationship does not hold true for the extended data set. As discussed above, our observations are likely related to the melt structure.

To evaluate the cause of the FWHM increase with decreasing alkalis in the basaltic glass subset, it is first necessary to examine the role of alkalis as charge compensators, network modifiers, or both. In the basaltic glasses, alkali charge compensation is required by Al³⁺ and Fe³⁺, but Al₂O₃ has near-constant concentrations and Fe³⁺ does not display a detectable effect on the melt structure, as discussed above. Therefore, the concentration of alkalis acting as charge compensators is likely near-constant in our basaltic glass subset. Thus, the increase in FWHM (that is caused by an increase of the intensity of the shoulder at ~1150–1230 cm⁻¹) with decreasing alkali content is likely related to decreasing modification of the silicate network by the alkalis. In other words, in glasses with near-constant Al₂O₃, a decrease in the amount of alkali network modifiers results in higher average Qⁿ, higher polymerization, and lower average Si-O bond distances, resulting in higher FWHM (or more contribution from the ~1220 cm⁻¹ shoulder).

For the extended data set of glasses, a negative correlation is not observed between the FWHM (i.e., intensity of the ~1220 cm⁻¹ shoulder) and the alkali content (Table 3b). The 11 non-basaltic glasses in the extended data set have a wide range of composition (SiO₂ = 55.16–80.17 wt%, Al₂O₃ = 11.93–28.52 wt%, and total alkalis = 3.94–16.93 wt%). Therefore, in these glasses with a large range in Al₂O₃ contents, it is probable that the percent of alkalis acting as charge compensators vs. network modifiers varies widely. The variable structural role of the alkalis in the 11 non-basaltic glasses in the extended data set likely contributes to the lack of negative correlation between alkali content and FWHM.

The 11 non-basaltic glasses in the extended data set also show a systematic shift of the ~1220 cm⁻¹ shoulder to higher wavenumbers with increasing SiO₂ content and decreasing Al₂O₃ content (e.g., Dalby et al. 2006; King et al. 2008; Dalby et al. in prep.). These observations indicate that there should be a systematic shift of the ~1220 cm⁻¹ shoulder to lower wavenumbers as Al becomes a more dominant network former [increasing molar Al/(Al+Si), which is indeed the case; Fig. 8]. Our findings are supported by observations in alkali aluminosilicate glasses, where decreasing Al/(Al+Si) results in lower average Si-O bond distances (Neuvill and Mysen 1996), which equates to higher average Qⁿ, higher polymerization, resulting in the ~1220 cm⁻¹ shoulder shifting to higher wavenumbers.

In the basaltic compositional range, however, where Al/(Al+Si) is near-constant, such a relationship between the ~1220 cm⁻¹ shoulder and Al/(Al+Si) or SiO₂ content is not ob-

served (FWHM; Table 3a; Fig. 6). In this case, the alkalis have a role as network modifiers, as discussed above.

Application of our results to emission and directional reflectance IR techniques

Our results, using KK transformation of specular reflectance spectra, show that the KK abs. peak location is related to the SiO₂ content in a wide range of glass compositions (47.2–80.2 SiO₂ wt%), and that the alkali content may be determined using the FWHM in basaltic glasses. We hypothesize that our KK absorbance results are directly applicable to IR studies using emission and directional reflectance.

Due to the fact that crystalline materials have polarization effects, the specular reflectance spectra of minerals may not be simply related to emission spectra. However, a glass does not have a crystalline structure and therefore its specular reflectance spectrum samples a random arrangement of molecular vibrations. Specular reflectance spectra of quartzofeldspathic glasses (Byrnes et al. 2007) are related to emission spectra in a manner similar to Kirchhoff's Law for directional reflectance spectra (R) (emission = 1 – R; Nicodemus 1965). This finding suggests that our results should be directly applicable to both emission spectra as well as directional reflectance spectra. Further studies that examine the KK transformation of specular, directional, and emission spectra of glasses are required to test our hypothesis.

Finally, our study shows that even small compositional changes may influence the IR peak location and FWHM. Emission and directional reflectance IR techniques analyze bulk rocks (>2 mg sample of glass ± minerals) and are commonly deconvolved with spectral databases that contain limited glass compositions (≤4 glasses). We suggest that to obtain the most information from such IR studies on glassy materials, it is beneficial to obtain electron microprobe analyses and backscattered electron (BSE) images of the materials. Those analyses may allow the researcher to determine if: (1) the spectral database glasses are appropriate compositions for models, and (2) the spectral deconvolution is consistent with the modal % minerals identified using the BSE images. Furthermore, studies that combine micro-reflectance FTIR with bulk techniques (emission

and directional reflectance) may provide further insight into the spectral features associated with glasses.

CONCLUDING REMARKS

The results of this study provide information that will help to better constrain mid-IR spectra of basaltic glasses and will aid in determining compositions of basaltic glasses; in particular, the SiO₂ and alkali contents. The trends identified in this study indicate that spectral databases should include glasses that are SiO₂-rich and SiO₂-poor, combined with alkali-rich and -poor compositions.

This study shows that the KK abs. peak location shifts to higher wavenumbers as SiO₂ content increases (KK abs. peak location = $2x + 938$, where $x = \text{SiO}_2 \text{ wt\%}$ for SiO₂ = 47.18–55.57 wt%). Also, we show that FeO_{total} and Fe³⁺/Fe²⁺ have negligible effect on mid-IR spectral features; therefore, mid-IR spectra may be used to determine SiO₂ and alkali contents in basaltic glasses with a wide range of FeO_{total} (6.06–16.30 wt%) and Fe³⁺/Fe²⁺ (0.05 to 1.17). We recommend that FeO_{total} and Fe³⁺/Fe²⁺ be examined using UV-visible-near-IR spectra where features specifically attributed to Fe electronic transitions are present (Bell and Mao 1976; Kakkadapu et al. 2003).

Our results are the first to show that the KK absorbance mid-IR spectra of basaltic glasses (47–56 SiO₂ wt%) have FWHM that decrease as alkali content increases, following FWHM (cm⁻¹) = $-13x + 235$ where $x = \text{alkali wt\%}$. This correlation occurs because Al/(Al+Si) is near-constant in the basaltic glass subset; therefore, the alkalis have a major role in modifying the basaltic glass network. If Al/(Al+Si) is not constant, then the IR band position and FWHM are dominantly controlled by changes in Al/(Al+Si) or SiO₂ content in natural silicate glasses.

ACKNOWLEDGMENTS

G. Poirier at the Canadian Museum of Nature is thanked for providing the electron microprobe analyses. D. Lui and J. Lockard synthesized basaltic glasses used in this study. Discussions with B. Hyde and M. Izawa are appreciated. This manuscript was significantly improved by helpful reviews by V.E. Hamilton and an anonymous reviewer. This work was supported by funds to P.L.K. from the Canadian Foundation for Innovation, Ontario Innovation Trust, Canadian National Science and Engineering Research Council and the Canadian Space Agency Space Science Enhancement Program.

REFERENCES CITED

- Agarwal, A., Davis, M., and Tomozawa, M. (1995) A simple IR spectroscopic method for determining fictive temperature of silica glasses. *Journal of Non-Crystalline Solids*, 185, 191–198.
- Angeli, F., Delaye, J.-M., Charpentier, T., Petit, J.-C., Ghaleb, D., and Faucon, P. (2000) Influence of glass chemical composition on the Na-O bond distance: a ²³Na 3Q-MAS NMR and molecular dynamics study. *Journal of Non-Crystalline Solids*, 276, 132–144.
- Basaltic Volcanism Study Project (1981) *Basaltic volcanism on the terrestrial planets*, 1286 p. Pergamon, New York.
- Bell, P.M. and Mao, H.K. (1976) Optical spectra and electron paramagnetic resonance of lunar and synthetic glasses: A study of the effects of controlled atmosphere, composition, and temperature. *Proceedings Lunar Science Conference*, VII, 2543–2559.
- Bell, R.J., Bird, N.F., and Dean, P. (1968) The vibrational spectra of vitreous silica, germania and beryllium fluoride. *Journal of Physics C: Solid State Physics*, 1, 299–303.
- Bingham, P.A., Parker, J.M., Searle, T., Williams, J.M., and Smith, I. (2002) Novel structural behaviour of iron in alkali-alkaline-earth-silica glasses. *Comptes Rendus Chimie*, 5, 787–796.
- Byrnes, J.M., Ramsey, M.S., King, P.L., and Lee, R.J. (2007) Thermal infrared reflectance and emission spectroscopy of quartzofeldspathic glasses. *Geophysical Research Letters*, 34, L01306.
- Calas, G., Henderson, G.S., and Stebbins, J.F. (2006) Glasses and melts: Linking

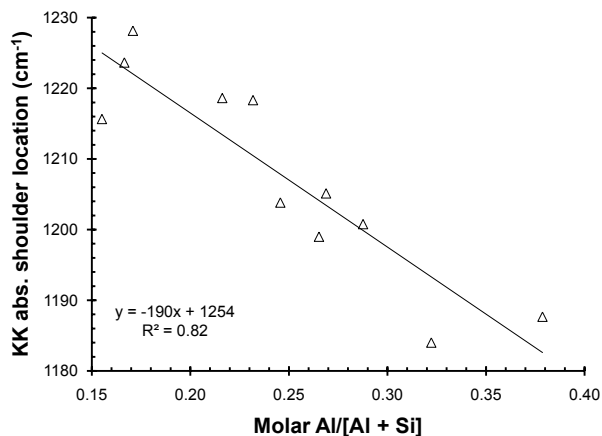


FIGURE 8. KK abs. shoulder location vs. molar Al/(Al+Si) for 11 non-basaltic glasses (King et al. 2008; Dalby et al. in prep.). Wavenumbers have an error of $\pm 2 \text{ cm}^{-1}$.

- geochemistry and materials science. *Elements*, 2, 265–268.
- Christensen, P.R., Bandfield, J.L., Smith, M.D., Hamilton, V.E., and Clark, R.N. (2000) Identification of a basaltic component on the Martian surface from thermal emission spectrometer data. *Journal of Geophysical Research*, 105, 9609–9621.
- Clark, R.N. (1999) Chapter 1: Spectroscopy of rocks and minerals, and principles of spectroscopy. In A.N. Rencz, Ed., *Manual of Remote Sensing*, Volume 3, Remote Sensing for the Earth Sciences, p. 3–58. Wiley, New York.
- Crisp, J., Kahle, A.B., and Abbott, E.A. (1990) Thermal infrared spectral character of Hawaiian basaltic glasses. *Journal of Geophysical Research*, 95, 21657–21669.
- Dalby, K.N. and King, P.L. (2006) A new approach to determine and quantify structural units in silicate glasses using micro Fourier-Transform Infrared spectroscopy. *American Mineralogist*, 91, 1783–1793.
- Dalby, K.N., Dufresne, C.D.M., King, P.L., Byrnes, J.M., Lee, R.J., and Ramsey, M.S. (2006) Characterization of glasses using infrared spectroscopy. *Geochimica et Cosmochimica Acta Supplement*, 70, 125.
- De Maeyer, E.A.P., Verbeeck, R.M.H., and Vercruyse, C.W.J. (2002) Infrared spectrometric study of acid-degradable glasses. *Journal of Dental Research* 81, 552–555.
- Domine, F. and Piriou, B. (1983) Study of sodium silicate melt and glass by infrared reflectance spectroscopy. *Journal of Non-Crystalline Solids*, 55, 125–130.
- Donaldson, C.H. (1979) Composition changes in a basalt melt contained in a wire loop of Pt₉₀Rh₁₀: effects of temperature, time, and oxygen fugacity. *Mineralogical Magazine*, 43, 115–119.
- Dowty, E. (1987) Vibrational interactions of tetrahedra in silicate glasses and crystals: I. Calculations on ideal silicate-aluminate-germanate structural units. *Physics and Chemistry of Minerals*, 14, 80–93.
- Efimov, A.M. (1996) Quantitative IR spectroscopy: Applications to studying glass structure and properties. *Journal of Non-Crystalline Solids*, 203, 1–11.
- Engelhardt, G. and Michel, D. (1987) High-Resolution Solid-State NMR of Silicates and Zeolites, p. 76. Wiley, New York.
- Furukawa, T., Fox, K.E., and White, W.B. (1981) Raman spectroscopic investigation of the structure of silicate glasses. III. Raman intensities and structural units in sodium silicate glasses. *Journal of Chemical Physics*, 75, 3226–3237.
- Grove, T.L. (1981) Use of FePt alloys to eliminate iron loss problem in 1 atmosphere gas mixing experiments: theoretical and practical considerations. *Contributions to Mineralogy and Petrology*, 78, 298–304.
- Guillot, B. and Sator, N. (2007) A computer simulation study of natural silicate melts. Part I: Low pressure properties. *Geochimica et Cosmochimica Acta*, 71, 1249–1265.
- Heaton, H.M. and Moore, H. (1957) A study of glasses consisting mainly of the oxides of elements of high atomic weight. Part II. The sources of the infrared absorption bands observed in the transmission curves of the glasses. *Journal of the Society of Glass Technology*, 41, 28–71.
- Henderson, G.S. (2005) The structure of silicate melts: A glass perspective. *The Canadian Mineralogist*, 43, 1921–1958.
- Holloway, J.R. and Burnham, C.W. (1972) Melting relations of basalt with equilibrium water pressure less than total pressure. *Journal of Petrology*, 13, 1–29.
- Hunt, J.M., Wisherd, M.P., and Bonahm, L.C. (1950) Infrared absorption spectra of minerals and other inorganic compounds. *Analytical Chemistry*, 22, 1478–1497.
- Johnson, J.R., Horz, F., and Staid, M.I. (2003) Thermal infrared spectroscopy and modeling of experimentally shocked plagioclase feldspars. *American Mineralogist*, 88, 1575–1582.
- Johnson, J.R., Staid, M.I., and Kraft, M.D. (2007) Thermal infrared spectroscopy and modeling of experimentally shocked basalts. *American Mineralogist*, 92, 1148–1157.
- Kakkadapu, R.K., Li, H., Smith, G.L., Crum, J.D., Jeoung, J.-S., Poisl, W.H., and Weinberg, M.S. (2003) Mössbauer and optical spectroscopic study of temperature and redox effects on iron local environments in a Fe-doped (0.5 mol% Fe₂O₃) 18Na₂O-72SiO₂ glass. *Journal of Non-Crystalline Solids*, 317, 301–318.
- King, P.L., McMillan, P.F., and Moore, G.M. (2004) Infrared spectroscopy of silicate glasses with application to natural systems. In P. King, M. Ramsey, and G. Swayze, Eds., *Infrared Spectroscopy in Geochemistry, Exploration Geochemistry and Remote Sensing*, 33, p. 93–133. Mineralogical Association of Canada, Short Course Series, Québec.
- King, P.L., Dufresne, C.D.M., and Dalby, K.N. (2008) Role of SiO₂, total FeO, Fe²⁺/Fe³⁺ and alkalis in glasses on thermal infrared spectra: Implications for spectral fitting. *Lunar Planetary Science Conference XXXVIII*, Abstract 2256.
- Le Maitre, R.W., Ed. (2002) *Igneous Rocks: a classification and glossary of terms*, 2nd edition. Cambridge University Press, New York.
- Logan, L.M., Hunt, G.R., and Salisbury, J.W. (1975) The use of mid-infrared spectroscopy in remote sensing of space targets. In C. Karr Jr., Ed. *Infrared and Raman Spectroscopy of Lunar and Terrestrial Minerals*, p. 117–142. Academic Press, New York.
- McMillan, P. (1984) Structural studies of silicate glasses and melts—applications and limitations of Raman spectroscopy. *American Mineralogist*, 69, 622–644.
- McMillan, P.F. and Hofmeister, A.M. (1988) Infrared and Raman spectroscopy. In F.C. Hawthorne, Ed., *Spectroscopy Methods in Mineralogy and Geology*, 18, p. 99–159. Reviews in Mineralogy, Mineralogical Society of America, Chantilly, Virginia.
- McMillan, P. and Piriou, B. (1982) The structures and vibrational spectra of crystals and glasses in the silica-alumina system. *Journal of Non-Crystalline Solids*, 53, 279–298.
- McMillan, P. and Wolf, G. (1995) Vibrational spectroscopy of silicate liquids. In J. Stebbins, P. McMillan, and D. Dingwell, Eds., *Structure, Dynamics and Properties of Silicate Melts*, 32, p. 247–315. Reviews in Mineralogy, Mineralogical Society of America, Chantilly, Virginia.
- McMillan, P.F., Grzechnik, A., and Chotalla, H. (1998) Structural characterization of SiO₂-CsAlO₂ and SiO₂-RbAlO₂ glasses. *Journal of Non-Crystalline Solids*, 226, 239–248.
- Merzbacher, C.I. and White, W.B. (1988) Structure of Na aluminosilicate glasses: A far-infrared reflectance spectroscopic study. *American Mineralogist*, 73, 1089–1094.
- Minitti, M.E., Mustard, J.F., and Rutherford, M.J. (2002) Effects of glass and oxidation on the spectra of SNC-like basalts: Applications to Mars remote sensing. *Journal of Geophysical Research*, 107, 5030, DOI: 10.1029/2001JE001518.
- Minitti, M.E., Lane, M.D., and Bishop, J.L. (2005) A new hematite formation mechanism for Mars. *Meteoritics and Planetary Science*, 40, 55–69.
- Minitti, M.E., Hamilton, V.E., and Wyatt, M.B. (2006) Investigation of the role of new glass compositions in remotely-sensed Martian lithologies. *Lunar Planetary Sciences Conference, XXXVII*, Abstract 2101.
- (2007) Deconvolution of Martian thermal infrared spectra using a simplified glass-rich library. *Lunar Planetary Sciences Conference, XXXVIII*, Abstract 2099.
- Moore, G., Chizmeshya, A., and McMillan, P.F. (2000) Calibration of a reflectance FTIR method for determination of dissolved CO₂ concentration in rhyolitic glass. *Geochimica et Cosmochimica Acta*, 64, 3571–3579.
- Mysen, B.O. (2006) The structural behavior of ferric and ferrous iron in aluminosilicate glass near meta-aluminosilicate joins. *Geochimica et Cosmochimica Acta*, 70, 2337–2353.
- Mysen, B.O. and Richet, P. (2005) *Silicate Glasses and Melts: Properties and Structure*, 544 p. Elsevier, New York.
- Neuville, D.R. and Mysen, B.O. (1996) Role of aluminum in the silicate network: In situ, high-temperature study of glasses and melts on the join SiO₂-NaAlO₂. *Geochimica et Cosmochimica Acta*, 60, 1727–1737.
- Nicodemus, F.E. (1965) Directional reflectance and emissivity of an opaque surface. *Applied Optics*, 4, 767–773.
- O'Neill, H.St.C. and Mavrogenes, J.A. (2002) The sulfide capacity and the sulfur content at sulfide saturation of silicate melts at 1400 °C and 1 bar. *Journal of Petrology*, 43, 1049–1087.
- Oskarsson, N., Sigvaldason, G.E., and Steinthorsson, S. (1982) A dynamic model of rift-zone petrogenesis and the regional petrology of Iceland. *Journal of Petrology*, 23, 28–74.
- Parot-Rajaona, T., Coté, B., Bessada, C., Massiot, D., and Gervais, F. (1994) An attempt to reconcile interpretations of atomic vibrations and ²⁹Si NMR data in glasses. *Journal of Non-Crystalline Solids*, 169, 1–14.
- Poe, B.T., McMillan, P.F., Angell, C.A., and Sato, R.K. (1992) Al and Si coordination in SiO₂-Al₂O₃ glasses and liquids: a study by NMR and IR spectroscopy and MD simulations. *Chemical Geology*, 96, 333–349.
- Salisbury, J.W. and Wald, A. (1992) The role of volume scattering in reducing spectral contrast of reststrahlen bands in spectra of powdered minerals. *Icarus*, 96, 121–128.
- Sweet, J.R. and White, W.B. (1969) Study of sodium silicate glasses and liquids by infrared reflectance spectroscopy. *Physics and Chemistry of Glasses*, 10, 246–251.
- Wyatt, M.B., Hamilton, V.E., McSweeney Jr., H.Y., and Christensen, P.R. (2001) Analysis of terrestrial and Martian volcanic compositions using thermal emission spectroscopy: I. Determination of mineralogy, chemistry, and classification strategies. *Journal of Geophysical Research*, 106, 14711–14732.
- Yoder, H.S. and Tilley, C.E. (1962) Origin of basalt magmas: an experimental study of natural and synthetic rock systems. *Journal of Petrology*, 3, 342–532.
- Zotov, N. and Keppler, H. (1998) The influence of water on the structure of hydrous sodium tetrasilicate glasses. *American Mineralogist*, 83, 823–834.